

# **Folding Large Graphene-on-Polymer Films Yields Laminated Composites with Enhanced Mechanical Performance**

*Bin Wang, Zhancheng Li, Chunhui Wang, Stefano Signetti, Benjamin V. Cunning, Xiaozhong Wu, Yuan Huang, Yi Jiang, Haofei Shi, Seunghwa Ryu, Nicola M. Pugno,\* Rodney S. Ruoff\**

Dr. B. Wang, Dr. C. Wang, Dr. B. V. Cuning, Dr. X. Wu, Dr. Y. Huang, Dr. Y. Jiang, Prof. R. S. Ruoff

Center for Multidimensional Carbon Materials  
Institute for Basic Science (IBS)  
Ulsan 44919, Republic of Korea  
Prof. R. S. Ruoff

Department of Chemistry and School of Materials Science and Engineering  
Ulsan National Institute of Science and Technology (UNIST)  
Ulsan 44919, Republic of Korea

E-mail: [rsruoff@ibs.re.kr](mailto:rsruoff@ibs.re.kr); [ruofflab@gmail.com](mailto:ruofflab@gmail.com)

Associate Prof. Z. Li, Prof. H. Shi  
Chongqing Institute of Green and Intelligent Technology,  
Chinese Academy of Sciences,  
Chongqing 400714, P. R. China

Dr. S. Signetti, Prof. S. Ryu  
Department of Mechanical Engineering  
Korea Advanced Institute of Science and Technology (KAIST)  
Daejeon 34141, Republic of Korea

Prof. N. M. Pugno  
Laboratory of Bio-inspired & Graphene Nanomechanics, Department of Civil, Environmental and Mechanical Engineering,  
University of Trento,  
Via Mesiano 77, 38123 Trento, Italy.

E-mail: [nicola.pugno@unitn.it](mailto:nicola.pugno@unitn.it)

Prof. N. M. Pugno  
School of Engineering and Materials Science,  
Queen Mary University of London,  
Mile End Road, London E1 4NS, U.K.

Prof. N. M. Pugno  
Ket-Lab, Edoardo Amaldi Foundation,  
Italian Space Agency,  
Via del Politecnico snc, 00133 Roma, Italy.

## **Abstract**

A folding technique is reported to incorporate large-area monolayer graphene films in polymer composites for mechanical reinforcement. Compared with the classic stacking method, the folding strategy results in further stiffening, strengthening, and toughening of the composite. By using a water–air-interface-facilitated procedure, an A5-size 400 nm thin polycarbonate (PC) film is folded in half 10 times to a  $\approx 0.4$  mm thick material (1024 layers). A large PC/graphene film is also folded by the same process, resulting in a composite with graphene distributed uniformly. A three-point bending test is performed to study the mechanical performance of the composites. With a low volume fraction of graphene (0.085%), the Young's modulus, strength, and toughness modulus are enhanced in the folded composite by an average of 73.5%, 73.2%, and 59.1%, respectively, versus the pristine stacked polymer films, or 40.2%, 38.5%, and 37.3% versus the folded polymer film, proving a remarkable mechanical reinforcement from the combined folding and reinforcement of graphene. These results are rationalized with combined theoretical and computational analyses, which also allow the synergistic behavior between the reinforcement and folding to be quantified. The folding approach could be extended/applied to other 2D nanomaterials to design and make macroscale laminated composites with enhanced mechanical properties.

**Keywords:** Graphene, folding, mechanical reinforcement, composites

Graphene oxide or reduced graphene oxide has seen wide use as a filler in composite materials as it can achieve significant mechanical enhancement with minimal volume of filling due to its mechanical properties and atomic thickness.<sup>[1-5]</sup> However, performance in some situations could be limited by defects (holes simply put) in the graphene oxide platelets. Furthermore, its incorporation in composite materials is typically with a random orientation that could limit mechanical reinforcement for certain applications when compared to having, say, platelets aligned in preferred directions.<sup>[6-10]</sup> Alternatively, the growth of large area, monolayer graphene on copper foils (by chemical vapor deposition, CVD) is now providing large, continuous, and high-quality graphene films, thus as a new candidate for mechanical reinforcement.<sup>[11-15]</sup> Incorporating large area but atomically thin monolayer CVD-grown graphene films into composite materials while simultaneously preserving their structure is essential to optimizing composite mechanics. Recently, inclusion of graphene monolayers into polycarbonate (PC)<sup>[16]</sup> or poly(methyl methacrylate) (PMMA)<sup>[17]</sup> composites at quite low volume fraction by a stacking approach resulted in a significant increase in elastic modulus, as measured by uniaxial tensile tests.

Here, to further strengthen the laminated composite, folding, rather than stacking of separated layers, is used to make a macroscale composite. Bending tests were used to measure the mechanical properties, while the combination of theoretical prediction and finite element method (FEM) numerical modeling allowed us to demonstrate and quantify the synergistic effect by both the presence of graphene and folding, on the enhancement of the reported mechanical properties. Having one continuous graphene

folded multiple times within the matrix yields a different type of structure with respect to simple matrix-graphene-stacked laminate with disconnected graphene layers. The fold plays a special role in stiffening and strengthening the composite. The folded structure can sustain a larger bending force as compared with the analog of stacked but disconnected layers, which could be explained by the improved layer–layer interaction generated from the additional constraint(s) by the folds.

In particular, the bending stiffness of a plate composed of  $n$  perfectly bonded layers of linear, elastic and isotropic material is<sup>[18]</sup>

$$D_n = \frac{E(nt)^3}{12(1-\nu^2)} = n^3 D_1 \quad (1)$$

where  $E$  is the Young's modulus of the material,  $\nu$  its Poisson's ratio and  $t$  the total thickness of the layer. Vice versa, for non-interacting layers, the total bending stiffness is by definition  $D_n = nD_1$ <sup>[18]</sup>. Thus in general  $D_n = n^\alpha D_1$  and we expect the following scaling for the nominal Young's bending modulus ( $\propto D_n/n^3$ )<sup>[18]</sup>

$$E_n \cong E_1 n^{\alpha-3} \quad (2)$$

where  $1 \leq \alpha \leq 3$  describes the interaction between the composite layers. Thus, the bending modulus of the laminated composites with and without folds is related to the interlayer interaction.

For the composite with a single layer graphene, the following rule of mixture holds

$$E_1 \cong E_g \frac{t_g}{t_g + t_m} + E_m \frac{t_m}{t_g + t_m} \quad (3)$$

where  $E_{g,m}$  are the graphene/matrix Young's moduli and  $t_{g,m}$  are the graphene/matrix thicknesses in the single layer with  $t_g + t_m = t$ . The two phases within a single layer are assumed to be perfectly bonded. Minimizing the value of  $t_m$  as well as maximizing

the interaction between the layers, i.e., the  $\alpha$  exponent, are the two strategies based on graphene composite folding for maximizing the bending modulus, with the theoretical value predicted to be

$$E_{1,\text{ideal}} \cong E_g \frac{t_g}{t_g + t_{m,\text{min}}} \quad (4)$$

and assuming  $E_g \gg E_m$ ,  $\alpha \rightarrow 3$  we expect  $t_{m,\text{min}}$  in the nanometer range (theoretically, for  $t_{m,\text{min}} = 0$  we obviously have  $E_{1,\text{ideal}} = E_g$ ). Equations 2 and 3 can be combined to predict a stiffening of the PC matrix due to the presence of the folding and graphene, according to

$$E_n^{(F,G)} = s_E f_E E_1 = s_E f_E g_E E_m \quad (5)$$

with  $f_E, g_E > 1$ , where  $f_E = n^{\alpha_f - \alpha}$  and  $\alpha_f$  denotes the exponent of Equation 2 in the presence of folding (larger than its non-folded counterpart  $\alpha$ ) and  $g_E = \frac{E_g}{E_m} \frac{t_g}{t_g + t_m} + \frac{t_m}{t_g + t_m}$  from Equation 3;  $s_E > 1$  is a factor which quantifies the mutual synergy between graphene reinforcement and folding process.

According to fracture mechanics<sup>[18]</sup> we expect a scaling of the delamination strength, which is responsible for the failure of our specimens and thus can be considered as the ultimate strength of the multilayer, as  $\sigma_u \propto \sqrt{E\gamma_C}$  where  $2\gamma_C$  is the fracture energy of the interface, also expected to depend on the presence of folding and/or graphene reinforcement, i.e.  $\gamma_C^{(F,G)} = \gamma_C s_\gamma f_\gamma g_\gamma$ , where  $s_\gamma, f_\gamma, g_\gamma > 1$  denote the related toughening mechanism due to folding and the graphene, respectively. The corresponding relations are shown as Equations S1–S3 in the Supporting Information. The synergy factors, which are defined analogously as for the bending modulus, account for further enhancement of different properties due to beneficial interaction of

reinforcement and folding process, as actually was observed in our experiments (see Table S1 in the Supporting Information). The previous equations will be applied for comparison with experimental values (see Table S2 in the Supporting Information).

To build a 3D material from 2D films by folding, paper origami provides a good example. It has been reported that A4 paper is difficult to fold (in half) more than 8 times, as the energy required for further folding increases rapidly.<sup>[19]</sup> Gallivan folded a 1200 m long sheet of paper in half 12 times.<sup>[19]</sup> To the best of our knowledge folding of nanoscale thin films many times has not yet been achieved. Very recently, we invented a method to realize 1 fold of monolayer CVD-grown graphene by using the surface of water to support the graphene; this method can be readily used for the folding of other large and thin 2D films.<sup>[20]</sup>

In this work, we folded  $\approx 400$  nm thick A5-sized ( $21\text{ cm} \times 15\text{ cm}$ ) PC films in half 10 times, yielding an  $\approx 0.4$  mm thick bulk “beam-like” sample with 1024 layers that had lateral dimensions of  $2.6\text{ cm} \times 0.11\text{ cm}$ . Through a simple modification of the procedure, PC on graphene films could be produced which, when folded, yielded a PC/graphene composite; a three-point bending test was then used to study the mechanical properties. Folding of either the pure PC film or the PC/graphene film resulted in enhanced mechanical properties compared to the nonfolded control samples. With a low volume fraction of graphene of 0.085%, the Young's modulus, strength, and toughness modulus were enhanced in the folded composite by an average of 73.5%, 73.2%, and 59.1%, respectively, as compared with the pristine stacked polymer films, or 40.2%, 38.5%, and 37.3% as compared with the folded polymer film.

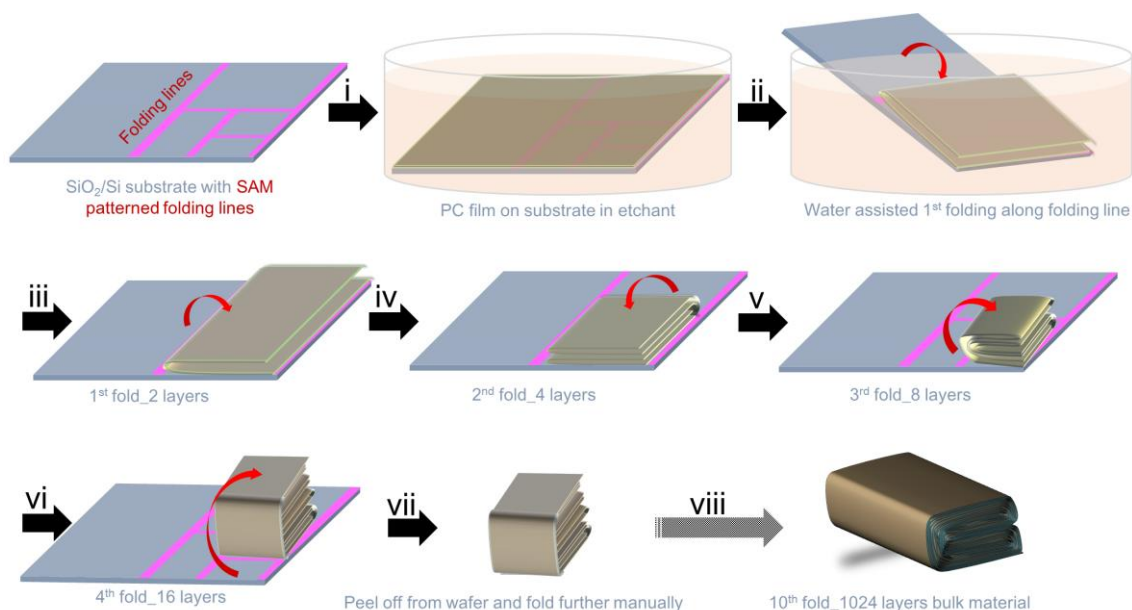


**Figure 1.** Schematic of the folding of an A5-sized  $\approx 400$  nm thick polycarbonate (PC) film, emphasizing the first four water-assisted folding steps that involve the use of a self-assembled-monolayer (SAM)-patterned substrate.

The process for achieving 10 folds using the thin film was divided into two distinct steps: first 4 folds are performed with a patterned “substrate to enable folding” and water-assisted delamination of the relevant part, and then 6 more folds were made by manually folding the film in half each time. The first step is shown schematically in **Figure 1**, with details in the Experimental Section. A silicon wafer piece (24 cm  $\times$  20 cm) with a 300 nm thick thermal oxide layer was modified with a hydrophobic self-assembled monolayer (SAM) and used as the substrate for the folding. The SAM pattern was designed with several “folding lines” for the initial 4 folds of the sample, as shown in Figure S1 (Supporting Information). As we have demonstrated previously, this hydrophobic SAM-modified substrate surface allows the polymer film to adhere to the hydrophobic region when immersed in water and enables folding when the

assembly is withdrawn from the water.<sup>[21]</sup> An A5-sized (21 cm length  $\times$  15 cm width  $\times$  25  $\mu\text{m}$  thick) polycrystalline Cu foil which had a PC layer spin-coated on its surface (PC–Cu) was then pressed onto this patterned substrate so that the substrate surface contacted with the PC layer. After etching away the Cu foil in aqueous etchant (0.2 M  $(\text{NH}_4)_2\text{S}_2\text{O}_8$ ) and replacing the etchant with deionized water, the assembly was slowly withdrawn from the water, and the floating PC film which was previously pressed on the hydrophilic region of the folding substrate (region without the SAM) folded over the other half of the PC film along the 1st folding line to realize the 1st fold. Three further folds were performed by the same water-assisted process to yield a 4-fold PC film with 16 layers, which had sufficient strength to be peeled from the substrate without damage for further manual folding. The steps of the folding process were recorded with photos, see Figure S2 (Supporting Information). After the 10th fold, the sample became too rigid to fold further. Then, it was compressed ( $\approx 40$  MPa) in a machine press at 150  $^\circ\text{C}$  for 10 min to improve interlayer contact, yielding the folded bulk material with thickness around 0.4 mm, consisting of a total of 1024 layers of thin film PC. To find out how many folds could be achieved, we found that the compressed 10-fold sample could be folded 2 more times (12 folds; Figure S3, Supporting Information). However, this 12-fold sample was not studied further due to the need for a minimum sample size in our mechanical testing equipment.

To incorporate CVD-grown graphene in the composite, the same folding procedure described above was used, however prior to PC spin-coating, the large copper foil was first coated with a continuous single layer graphene (G) grown by CVD,<sup>[12, 22]</sup> thus



producing a “**PCG**” film on the Cu foil. The thickness of a single layer **PCG** obtained by spin-coating a 4 wt% PC/chloroform solution on CVD-grown monolayer graphene film/Cu foil was measured using atomic force microscopy (AFM), as shown in Figure S4 (Supporting Information). The thickness is around 400 nm, which was the thinnest film for which we could reliably form the 1st fold of the A5-sized film without fracture in our experiments.

To compare the effect of folding (**F**) versus stacking (**S**), we also prepared samples by sequentially stacking individual layers of  $\approx 400$  nm thick PC both with (**S-PCG**) or without (**S-PC**) a single monolayer graphene film to compare their mechanical response to their folded counterparts, i.e., “**F-PCG**” or “**F-PC**” composites. Note that the **S-PCG** layers were stacked in a PC–G–G–PC sequence to maintain the same stacking order as the folded sample. All samples were hot pressed at 150 °C for 10 min at  $\approx 40$  MPa to densify the composite and promote the interfacial contact, prior to measurement at room temperature in ambient conditions.

Scanning electron microscopy (SEM) images in **Figure 2a,b** show the cross-section of **S-PCG**, where the closely stacked layered structure can be observed. A similar (appearing) layered structure is also observed in the cross-section of **F-PCG** in **Figure 2c**, and the thickness of both samples was about 0.4 mm. The fold structure of **F-PCG** is shown in **Figure 2d**, where the vertically aligned and curved layers can be clearly observed. As compared with the horizontally stacked layers, these densely stacked vertical layers at the fold provide an additional constraint to the in-plane relative slip and normal separation of the layers, allowing the sample to sustain a larger bending

force. **Figure 2e** shows the “continuously wrapped” configuration of the fold edge of the **F-PCG** sample, in comparison to the “open” layer edges in the case of **S-PCG** (**Figure 2a**). The volume fraction of graphene in the sample was estimated by accounting for the thickness of an individual layer of PC film, and the thickness of single layer graphene (assumed to be 0.34 nm) which yielded  $\approx 0.085$  vol% graphene.

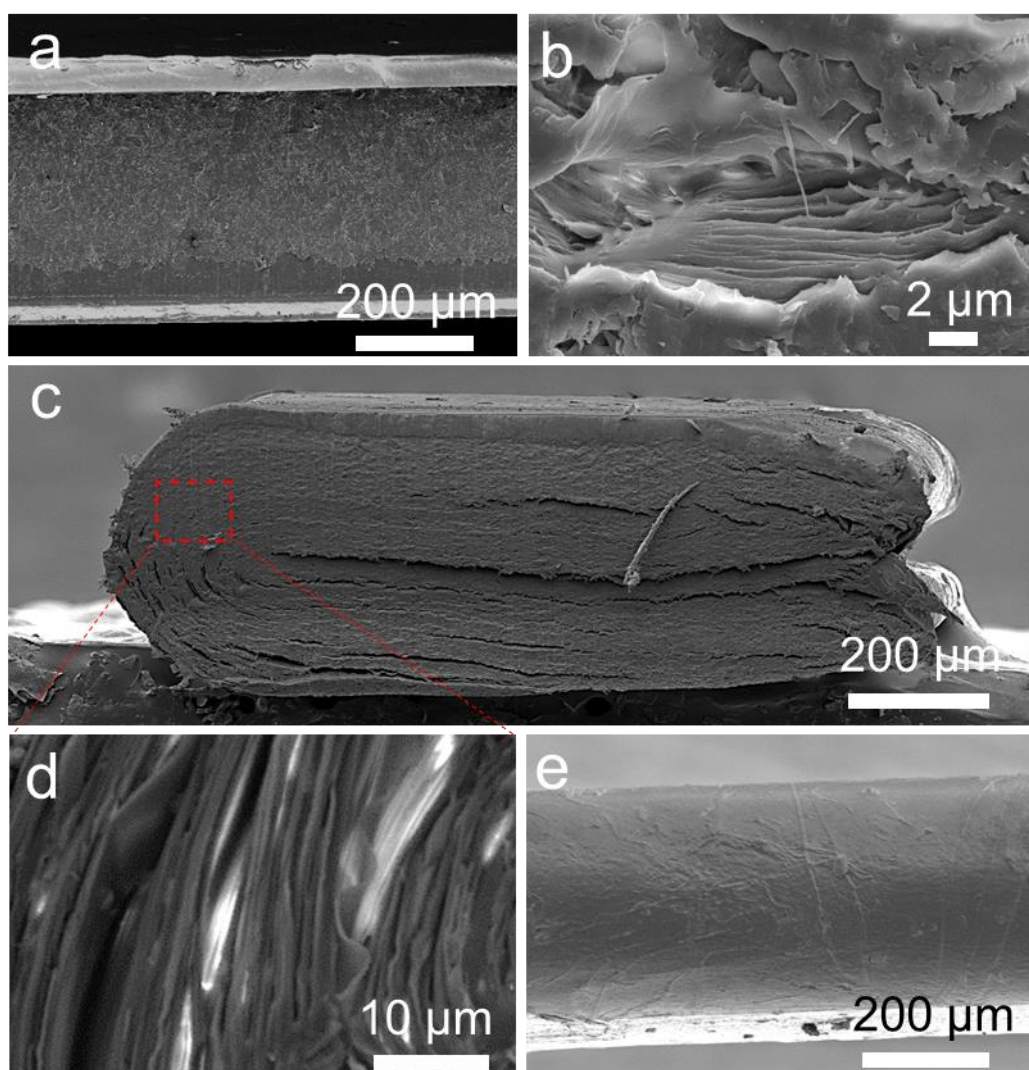


**Figure 2.** SEM images of the composite structures. (a,b) Cross-section of 1024 stacked layers of PCG film (**S-PCG**), and (c,d) cross-section of a **F-PCG** composite folded 10 times, and (e) the fold edge (left side of the sample in (c)).

To evaluate the graphene presence in the composites, Raman spectroscopy was used, see **Figure 3** and Figure S5 (Supporting Information). The characteristic bands of PC appear at 1234.9, 1607.2, and 3075.1  $\text{cm}^{-1}$ , representing the C-O, and methyl groups, respectively.<sup>[16]</sup> With a single layer of graphene film on top of the PC film, the G (1587.2  $\text{cm}^{-1}$ ) and 2D (2676.3  $\text{cm}^{-1}$ ) bands for graphene are observed with negligible D band ( $\approx 1350 \text{ cm}^{-1}$ ), indicating the high quality of the monolayer graphene film. The inset in **Figure 3a** highlights the position difference of the G band of graphene and the band of PC which can be used for distinguishing graphene from PC. **Figure 3b** compares the spectra from the “plane” regions of the four bulk composites, in which **S-PC** and **F-PC** show pure PC signals, while **S-PCG** and **F-PCG** exhibit strong features of both PC and graphene.  $I_{2D}/I_G$  maps for 1 layer **PCG**, **S-PCG**, and **F-PCG** are compared in Figure S5 (Supporting Information). The  $I_{2D}/I_G$  ratio of  $\approx 2$  across the map for 1 layer **PCG** indicates the monolayer character of the graphene film on PC.<sup>[23]</sup>  $I_{2D}/I_G$  values lower than 2 were observed in the maps for **S-PCG** and **F-PCG**, due to the twisted two graphene layers in these composites formed during the stacking and folding processes.<sup>[23]</sup> Low and comparable D bands were detected for both **S-PCG** and **F-PCG** composites, corresponding to the  $I_D/I_G$  maps shown in **Figure 3c,d**. Defects were generated during “handling” of the graphene films, but the low intensity of the D band suggests that both stacking and folding processes preserved the high quality of the graphene films. Besides the “plane” regions for the composites, graphene quality in the “edge” regions was also measured by Raman maps, as shown in **Figure 3e,f**. High  $I_D/I_G$  intensity across the entire “edge” region for **S-PCG** shows the defects from the edges

of graphene layers. In contrast, the graphene film is continuous at the fold of **F-PCG**, and thus low intensity of D band comparable to the “plane” region was observed in the “edge” region, indicating the high uniformity of graphene in **F-PCG**. Thus, folding process results in a multilayer composite with higher homogeneity of properties, avoiding the intrinsic weakness of edge regions.

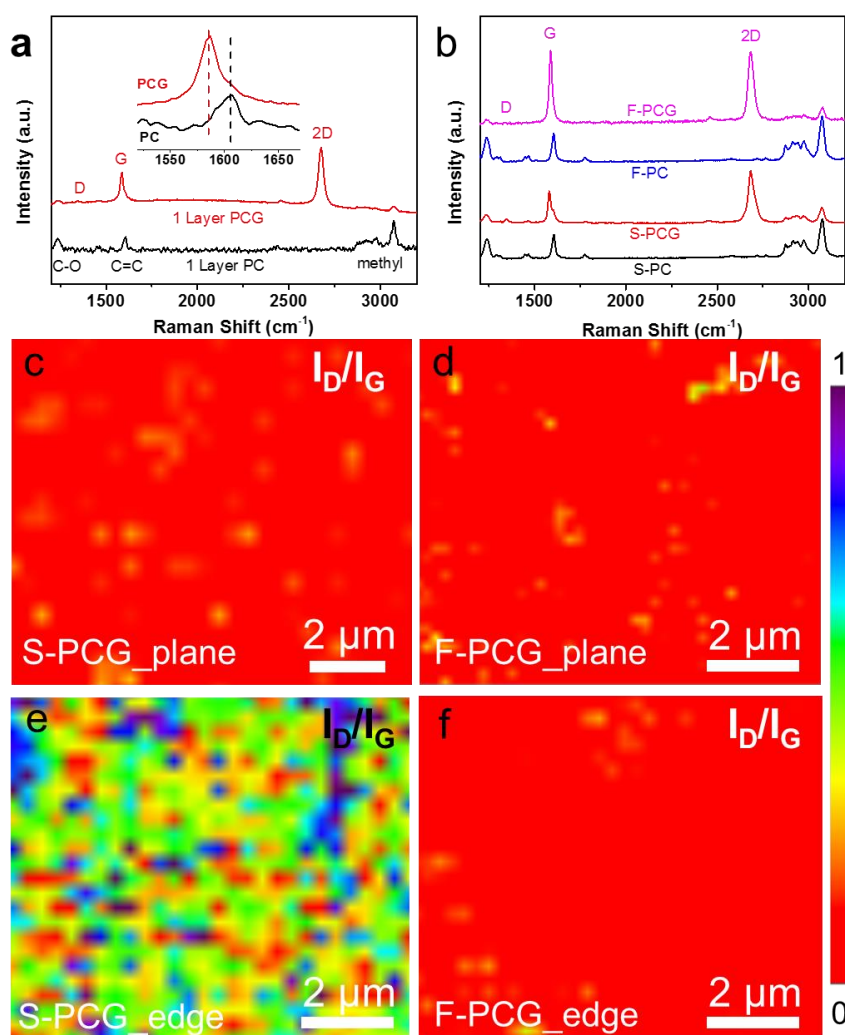


**Figure 3.** Raman spectroscopy of **S-PC**, **S-PCG**, **F-PC**, and **F-PCG** composites. (a) Raman spectra of single layers of **PC** and **PCG**. The inset shows that the G band position of graphene in **PCG** and the band of **PC** are distinguishable. (b) Comparison of Raman spectra of the “plane” regions for the four tested multilayers. (c–f) Raman maps of the intensity ratio of D to G bands ( $I_D/I_G$ ) in the “plane” regions (c,d), and “edge” regions for **S-PCG** and **F-PCG** (e,f).

To study the mechanical properties of the composite samples, bending tests were performed. A three-point bending configuration with a dynamic mechanical analysis (DMA) system was used, see Figure S6 (Supporting Information). The dimensions of the specimens were 15 mm × ≈1.1 mm × ≈0.4 mm (span × width × thickness, thus the span-to-thickness ratio is 37.5, based on the ASTM-D7264), and five specimens were measured for each composite configuration (Figure S7 and Table S2, Supporting Information). The loading tip had a cylindrical geometry and the radius was ≈0.3 mm. The length of the straight loading tip was 20 mm, much larger than the width of the specimens of 1.1 mm, resulting in a uniform contact with the specimen across its width. The maximum allowed deflection was 5 mm, thus the maximum strain resulting in the specimens was 5.3% (Equation 7). The stress–strain plots were obtained by fixing the ramp displacement rate to 100 μm min<sup>-1</sup> and measuring the applied force and deflection. In a three-point bending test, the failure of the specimen may occur due to either crack nucleation on the tensed surface (bottom chord) or to localized buckling and delamination or crushing at the compressed chord. The compressed chord of the beam is the surface that is in contact with the loading nose and thus opposite to the tensed chord. To convert the force–deflection to the stress–strain plot, the stress was calculated by

$$\sigma = \frac{3PL}{2bh^2} \quad (6)$$

where  $\sigma$  is the tensile stress at the bottom chord at mid-span,  $P$  is the external applied force, and  $L$ ,  $b$ , and  $h$ , are the span, width, and thickness of the beam, respectively. The strain was calculated as

$$\varepsilon = \frac{6\delta h}{L^2} \quad (7)$$

where  $\varepsilon$  is the tensile strain at the bottom chord of the beam, and  $\delta$  is the mid-span deflection. We used SEM to investigate the failure mechanism of the samples after bending tests, as shown in Figures S8 and S9 (Supporting Information). Cracks appeared on the tensed surface of the bent **S-PC** and **S-PCG** specimens, but no cracks were observed on the **F-PC** and **F-PCG** samples, indicating that the failure of the stacked samples was due to cracking of the tensed surface. On the other hand, no buckling was observed on the compressed surface for the **S-PC** and **S-PCG** specimens but appeared on the **F-PC** and **F-PCG** samples, indicating that the failure of the folded samples was due to buckling on the compressed surface.

The different failure mechanisms for the stacked and folded samples result from the different stress distributions from bending that arise by different layer interactions from the folding, as shown in **Figure 4a**. By employing FEM simulations, we modeled the bending behavior of 4-fold, 5-fold, and 6-fold PC samples as compared with the corresponding stacked samples of 16 layers, 32 layers, and 64 layers. It was infeasible to directly model the 10-fold sample due to the high computational cost and the complexity in defining the boundary conditions to replicate folds (see the Experimental Section). Still, the simulation results enabled us to understand the effect of folding on the scaling of bending properties. As depicted in **Figure 4a**, the folded configuration provides much higher bending stiffness with respect to the stacked configuration due to the additional constraint given by the folds which results in enhanced layer mechanical interaction. This, consequently, results in both higher specific deformation

energy stored in the plate, and also higher bending force (see Figure S10 in the Supporting Information) at the same imposed displacement. The effective stress on the folded regions (located at the edges and in the center of the samples) is approximately an order of magnitude higher than the stress in the mid-span of the stacked samples that is spread uniformly across the width of the sample. This higher effective stress is reflected on the load bearing capacity of the different layering configurations. A peripheral (at the sample edges) constraint due to folding allows the top layers to work in compression (as in a homogeneous bent beam), and the top layer is eventually delaminated and undergoes wrinkling. The simulation captures similar behavior observed in experiments (Videos S2, S4, and S6, Supporting Information). As a result, a much larger force and deformation energy are required to bend the folded samples with respect to the stacked samples, as depicted in **Figure 4b,c**.

In the stacked samples, the specific bending force and deformation energy are nearly constant irrespective of the number of layers, while they significantly increase with the number of layers for the folded samples (Figure S10, Supporting Information). By computing the bending stiffness of **S-PC** and **F-PC**, we extract the exponent  $\alpha_{\text{F-PC}} = 2.251$  that, in agreement with the theoretical prediction, lies in between the two limit cases of  $\alpha_{\text{S-PC}} = 1$  (no bonding and actually observed in simulations of **S-PC** with different  $n$ , **Figure 4b**) and  $\alpha = 3$  (perfect bonding/homogeneous beam). The exponent  $\alpha_{\text{F-PC}} = 2.251$  is closer to the latter, demonstrating that folding is an effective strategy to produce a multilayer sample with enhanced mechanical properties closer to the limit of a perfectly homogeneous beam. Similar results are found by

analyzing the deformation energy stored by the simulated samples. Since the internally stored energy at a given deflection  $\delta$  is proportional to the product of the external applied force and the deflection,  $T_n \propto P \cdot \delta$ , and the force at a given deflection scales with  $n^\alpha$  (the same as the bending stiffness, see Equation 1), we expect similar scalings between the beam internal deformation energy and bending stiffness. In agreement with this prediction, the power-law behavior is clearly observed also for the strain energy and the related extracted exponents are  $\alpha_{S-PC} = 1.148$  and  $\alpha_{F-PC} = 1.828$ , which are comparable to those determined from the bending stiffness. The observed difference is attributed to the fact that the deformation energy is affected by contact pressure at support/load points that increases with the stiffness of the beam. Also, the interface behavior is affected as the presence of folds increases the energy dissipated by friction (nearly 1/10 of the corresponding deformation energy, Figure S10, Supporting Information). This can be directly correlated to the complex relative displacement between layers induced by the fold constraints (**Figure 4a** and Videos S2, S4, and S6 (Supporting Information)), indicating that the tailoring of interface parameters could further increase the load bearing capacity toward the ideal bulk beam value.



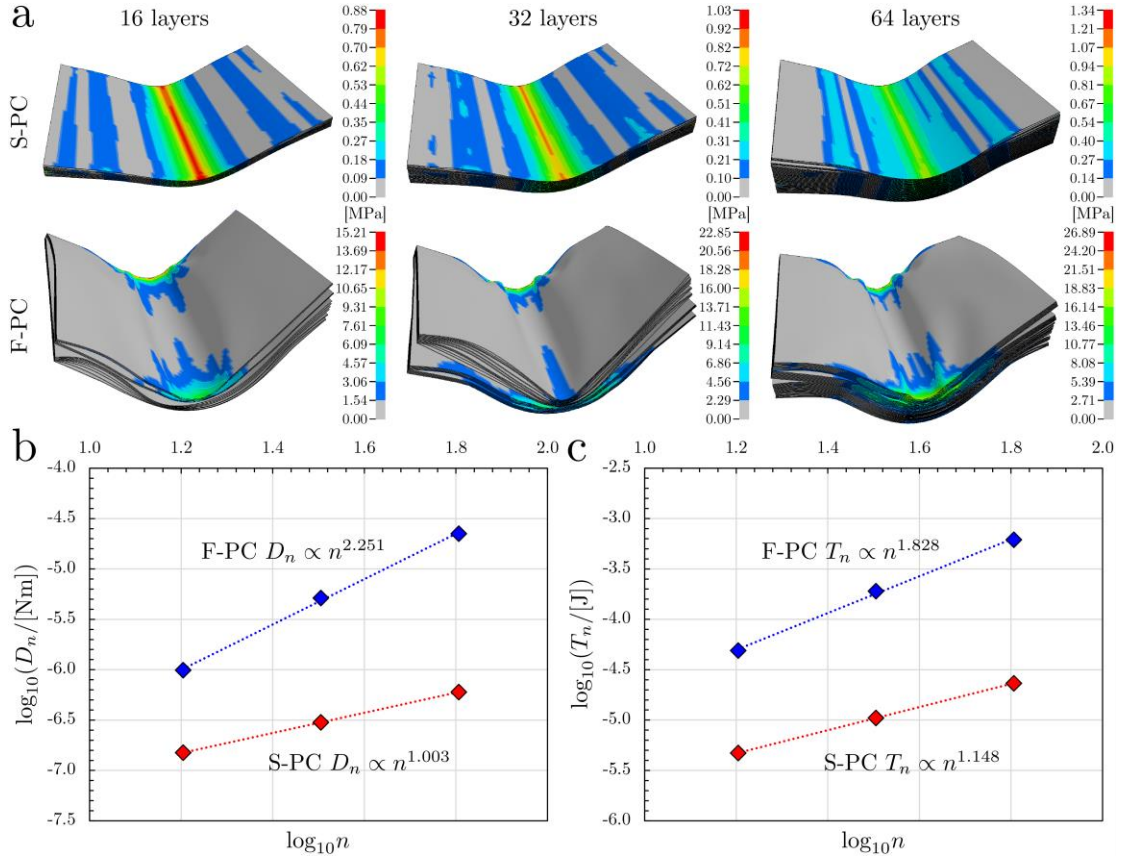


**Figure 4.** FEM three-point bending simulations on **S-PC** and **F-PC** samples, with  $n = 16$  (4 folds), 32 (5 folds), and 64 (6 folds), aimed at discriminating the mechanical role of folding on the multilayer bending properties. a) Visual comparison of bending behavior of the samples with a contour plot of the von Mises stress within the specimen (units: MPa). Animations of the simulations are provided in Videos S1–S6 (Supporting Information). (b) Numerical scaling of the bending stiffness  $D_n \propto n^\alpha$  (secant at 1 mm deflection), from where the theoretical power-law scaling dependencies are confirmed and the  $\alpha, \alpha_f$  power exponents can be extracted. (c) Scaling of the specific deformation energy  $T_n$  (at 1 mm deflection). Complete simulation results (bending force, deformation energy, sliding interface energy) are reported in Figure S10 (Supporting Information).

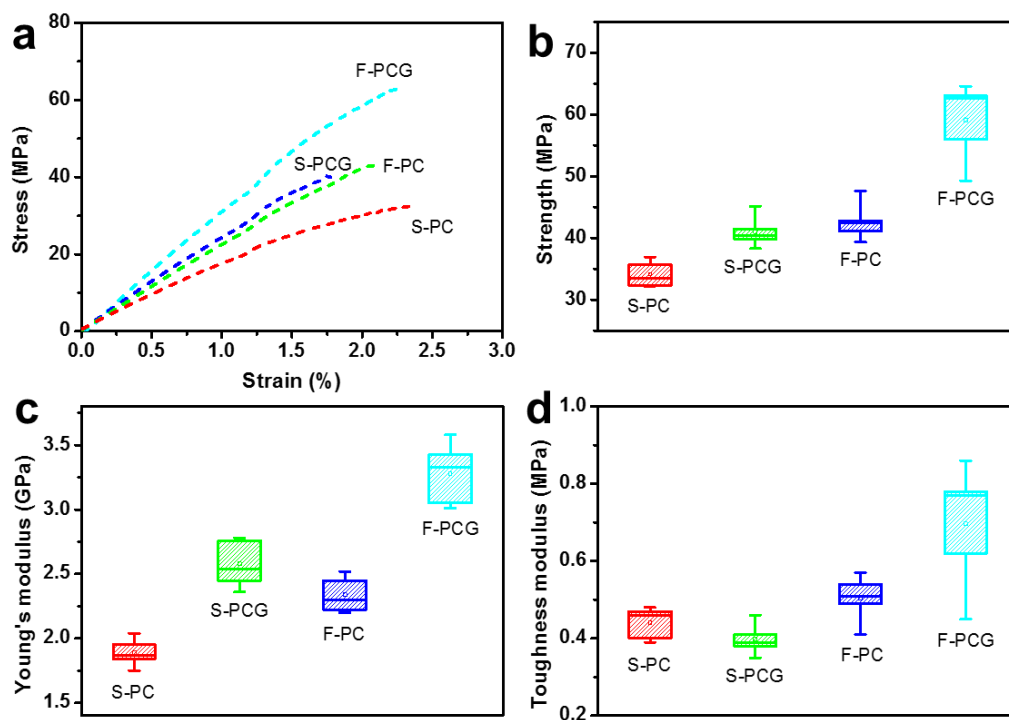


**Figure 5.** Mechanical test for the composites using three-point bending performed on dynamic mechanical analysis (DMA) equipment. (a) Typical stress–strain responses under loading for different composites including **S-PC**, **S-PCG**, **F-PC**, and **F-PCG**. (b–d) Statistic of fracture strength (b), Young's modulus (c), and toughness modulus (d) of different composites measured in ambient conditions. Five specimens were measured for each composite, and the summary of the as-measured mechanical properties is reported in Table S2 (Supporting Information), including maximum and average values also for the fracture strain. Note the superior mechanical characteristics for both maximum and average values of the **F-PCG** solution (with the exception of the fracture strain, see Figure S11, Table S2, and the “Model Predictions” section in the Supporting Information).

By comparing the stress–strain curves for **F-PC** and **S-PC** (Figure 5a), it was found that the folded composite showed an average (maximum) strength of  $42.65 \pm 3.08$  MPa (47.61 MPa), which is higher than strength for the stacked composite of  $34.12 \pm 2.10$  MPa (36.91 MPa), thus a larger load is required to fracture the **F-PC** composite (Figure

5b). A similar trend was observed in the cases for **F-PCG** and **S-PCG**, with strength, respectively, of  $59.08 \pm 6.41$  MPa (64.56 MPa) and  $41.03 \pm 2.58$  MPa (45.16 MPa), indicating that the difference in mechanical performance should depend on the difference in the structure of the composites, thus folded versus the stacked. The average (maximum) Young's modulus was: **F-PC** of  $2.34 \pm 0.14$  GPa (2.52 GPa) versus **S-PC** of  $1.89 \pm 0.11$  GPa (2.04 GPa), and **F-PCG** of  $3.28 \pm 0.24$  GPa (3.58 GPa) versus **S-PCG** of  $2.58 \pm 0.19$  GPa (2.78 GPa), see **Figure 5c**. The folded composite is much stiffer than the stacked composite. The toughness modulus between samples was obtained as the area under the stress–strain curve. In **Figure 5d**, the folded samples have larger average (maximum) toughness modulus values of  $0.70 \pm 0.16$  MPa (0.86 MPa) for **F-PCG** and  $0.51 \pm 0.06$  MPa (0.57 MPa) for **F-PC** than the stacked samples ( $0.40 \pm 0.04$  MPa (0.46 MPa) for **S-PCG** and  $0.44 \pm 0.04$  MPa (0.48 MPa) for **S-PC**). The fracture strain values are comparable for all the samples, as shown in Figure S11 (Supporting Information).

Besides the benefits from folding the PC film alone, filling with graphene further improves the mechanical performance of the composites. Despite the low volume fraction of 0.085% for graphene in the composites, the average (maximum) Young's modulus increased by 36.51% (36.27%) and 40.17% (42.06%) respectively for **S-PCG** and **F-PCG**. By considering both the effects from folding and graphene filling, the Young's modulus, strength, and toughness modulus were enhanced by an average of 73.5%, 73.2%, and 59.1%, respectively, for the **F-PCG** composite as compared with **S-PC**, or 40.2%, 38.5%, and 37.3% as compared with **F-PC**, by considering only the

reinforcement effect on the folded composite from graphene. We highlight this synergy by back-calculating the equivalent Young's modulus of the reinforcement  $E_g$  from rule of mixture of Equation 3 by exploiting experimental results (Table S2, Supporting Information). Assuming  $E_m = 1.89$  GPa (average modulus from bending test on S-PC) from S-PCG samples (average  $E_1 = 2.58$  GPa) we derive  $E_g = 0.81$  TPa, which is comparable with the measured values for graphene as reported previously,<sup>[24-26]</sup> and  $E_g = 1.64$  TPa from F-PCG samples (average  $E_1 = 3.28$  GPa). The latter value, which is somewhat higher than the ideal modulus of graphene ( $\sim 1$  TPa), clearly quantifies the contribution given by the folding process in improving the mechanical properties of such nanocomposites. Similarly, for the back-calculated graphene strengths we found 8.17 GPa in absence of folding and 29.42 GPa in the presence of folding, again a significant fraction of the graphene ideal strength ( $\sim 100$  GPa).

As a control experiment, we prepared a **PCG** sample using a melt process (**Melt-PCG**). Briefly, a PCG film of the same dimensions as those used in the stacked and folded samples was crumpled and then melted on a hot plate at 300 °C. Using the same thickness for the film ensured the same graphene-to-polymer ratio of the stacked and folded multilayers. After cooling, the PC/graphene melt was hot pressed (40 MPa) at 150 °C for 10 min to obtain films with a thickness of 0.4 mm. These films were then cut to obtain samples with the same beam geometry as the folded and stacked samples. The mechanical response of these samples are shown in (Figure S12, Supporting Information). The average values are: Young's modulus of  $2.29 \pm 0.18$  GPa, fracture strength of  $43.53 \pm 3.54$  MPa, and toughness modulus of  $0.54 \pm 0.07$  MPa (Table S3,

Supporting Information); these values are all much lower than those for **F-PCG**, further indicating the advantages of folding the embedded graphene over other established processes.

For a comparison between experiments and model predictions, we use Equation 5 and Equations S1–S3 (Supporting Information), finding a good agreement with  $f_E \cong 1.242$ ,  $g_E \cong 1.372$ ,  $f_\sigma \cong 1.254$  and  $g_\sigma \cong 1.208$ , see the “Model predictions” and Table S2 (Supporting Information). Such a model could thus guide the design of similar types of multi-layered composites. Finally, we note that the extracted value of  $g_E$  is in good agreement with the prediction of Equation 3 which yields  $g_E \cong 1.449$ , with  $E_m = 1.89$  GPa (average modulus from bending test on **S-PC**). From analysis of experimental tests with our model we also derived the global synergy factors  $s_E \cong 1.023$ ,  $s_\sigma \cong 1.146$ ,  $s_\varepsilon \cong 1.261$  and  $s_\gamma \cong 1.521$  which demonstrate and quantify how the reinforcing with 2D materials and the folding process mutually strengthen their contribution to further enhancing mechanical properties. Indeed, from our experiments, the average Young’s modulus for **S-PCG** and **F-PCG** are  $2.58 \pm 0.19$  GPa and  $3.28 \pm 0.24$  GPa, and the maximum values are 2.78 GPa and 3.58 GPa, respectively, which are higher than the prediction of a simple rule of mixture. Moreover, recalling that  $f_E = n^{\alpha_f - \alpha}$  we derive from experimental results (Table S2, Supporting Information)  $\alpha_f - \alpha = 0.0313$  and assuming the simulation derived scaling exponent ( $\alpha_f = 2.251$ ) we obtain  $\alpha = 2.222$ . This value cannot be compared with the nearly negligible value for **S-PC** samples from the simulations, where we have deliberately reduced all the layer–layer interactions – adhesive energy fixed to be null with layers (apart normal contact

and friction), which are nearly independent – to let the mere role of folding emerge. The low estimated exponent difference  $\alpha_f - \alpha$  indicates a limited effect of folding in tested specimens. This can be explained by the role of adhesive interaction: in tested **PCG** sample, the adhesion energy between the layers was also high in the stacked sample, hence the limited improvement, while in our simulations, the contribution of folds is consequently more evident. The results show how the contribution of folding is much more useful in case of weak interfaces, for example, to counteract the presence of impurities or size-scale effects on adhesive interactions (low ratio between surface and volume forces), e.g., for the production of large-scale composites. Thus, the fold effect could be understood as an enhanced layer–layer interaction as compared with the stacked layers, yielding improved mechanical properties.

Here we also note that the thickness of polymer and the number of graphene layers may also affect the mechanical properties of the composite. Theoretically, reducing the thickness of the polymer by a factor  $p$  and increasing the number  $q$  of graphene layers, considering for the Young's modulus of the graphene multilayer the same Equation 2 with an exponent  $\alpha_g$  ( $n \rightarrow q$ ), would result in  $g_E(p, q) \cong g_E(1, 1) \frac{p}{q^{2-\alpha_g}}$  ( $E_g \gg E_m, t_m \gg t_g$ ). Considering the intermediate value of  $\alpha_g \cong 2$ <sup>[18, 27]</sup> suggests that the number of graphene layers is not affecting the results and thus is not as important as the polymer thickness. For example, by reducing the polymer thickness by a factor of 4 would result in a stiffening by a factor of 4, a strengthening by a factor of 2, a reduction in the maximal strain by a factor of 2, and in an invariant toughness modulus. Therefore, the mechanical performance of the composite could be enhanced greatly by further

reducing the thickness of polymer layer, although we have already used the thinnest PC film of 400 nm that we could fold without damage in this work.

In summary, folding was demonstrated to be an effective way to embed graphene in a polymer composite for achieving a high homogeneous multilayer with enhanced mechanical properties, providing a more effective reinforcement to the composite than simply stacked layers. Beyond the extreme alignment between graphene and polymer layers that can be realized by stacking, folding provides extra constraint(s) within the plate, resulting in additional stiffening, strengthening, and toughening of the composite.

A water-based technique was used to fold an A5-sized polycarbonate film in half 4 times followed by manual folding 6 more times, from a single layer film of 400 nm thick to an  $\approx 0.4$  mm thick bulk material with 1024 layers. This method was also used to embed monolayer graphene film into a composite structure which also has 1024 layers and similar overall thickness, thus forming a new type of composite with graphene. Even with a low volume fraction of graphene of 0.085% in the folded composite, the Young's modulus, strength, and toughness modulus were enhanced by an average of 73.5%, 73.2%, and 59.1%, respectively, as compared with the pristine stacked polymer films. In the stacked samples, the incorporation of graphene resulted in the enhanced Young's modulus of 36.5%, strength of 20.3%, and comparable toughness moduli, while these enhancements were 40.2%, 38.5%, and 37.3%, respectively, in the folded samples with the same volume percentage of graphene. The contribution of graphene reinforcement was thus increased by the folding, indicating a synergistic reinforcement mechanism from both folding and graphene, as quantified by

the synergy factors. The models presented in this work could be helpful for the design of 2D material embedded in multilayered 3D composites, which can be realized at large size such as the experimental methods described in this work. Our synergistically enhanced graphene-reinforced composites made by folding are able to exploit the ideal properties of graphene and could thus be potentially applied on large scale in the aerospace and automotive industries. Furthermore, by combining various 2D materials that contribute special functionality, folding can be used to obtain macroscale materials for many other potential applications, including, but not limited to, energy storage and conversion, and thermal management.

## **Experimental Section**

**Patterning substrate SAMs:**  $\text{CF}_3(\text{CF}_2)_5(\text{CH}_2)_2\text{SiCl}_3$  (trichloro(1*H*,1*H*,2*H*,2*H*-perfluorooctyl)silane), was used to form a SAM pattern on a silicon wafer (24 cm × 20 cm) having a 300 nm thick thermally oxidized surface. The  $\text{SiO}_2/\text{Si}$  substrate was first exposed to  $\text{O}_2$  plasma for 10 min to modify the surface with silanol groups (-Si-OH) for further reaction with  $\text{CF}_3(\text{CF}_2)_5(\text{CH}_2)_2\text{SiCl}_3$ , then PET films were used as masks to cover the surface regions where no modification by SAM was wanted.  $\text{CF}_3(\text{CF}_2)_5(\text{CH}_2)_2\text{SiCl}_3$  (50  $\mu\text{L}$ ) was added to a vial and put into a vacuum desiccator together with the wafer and left for 12 h at room temperature to deposit the SAM molecules on those regions not covered by PET film. Then, the PET film regions were peeled from the wafer and those regions not covered by PET film formed a SAM pattern (hydrophobic) with the other hydrophilic regions. The patterned substrate was rinsed



with ethanol and dried with nitrogen before use. The pattern design is shown in **Figure 1** and Figure S1 (Supporting Information).

**Folding process:** The 10 times folding process was divided to two steps: the first 4 folds were achieved by the transfer/folding on water using the patterned substrate, and then 6 more folds were done manually. A 4 wt% PC/chloroform solution was spin-coated on an A5-sized (21 cm × 15 cm) Cu foil at 5000 rpm to form a PC film with thickness of about 400 nm. PC used here was poly(bisphenol A carbonate) from Sigma-Aldrich (average  $M_w \approx 45\ 000$ ). Then, the PC-coated Cu foil (**PC-Cu**) was pressed onto the patterned substrate so that the substrate surface contacted the PC layer. After etching away the Cu foil in the aqueous etchant (0.2 mol ammonium persulfate) and replacing the etchant with pure water, the assembly was slowly withdrawn from water, and the floating PC film (that had been on the hydrophilic region (no SAM region)) was folded over the other half of the PC film along the 1st folding line, to realize the 1st fold. The next 3 folds were achieved one after another by the same water-assisted process to get a PC film with 16 layers; by trial-and-error procedure we found that this was strong enough to be peeled off from the substrate without (apparent) damage for further folding “by hand.” After the 10th fold, the sample was too rigid to be folded further. This 1024-layer sample made in this manner from the original 400 nm thick PC film was compressed ( $\approx 40$  MPa) in a machine press with a couple of stainless steel spacers with thickness of 0.4 mm at 150 °C for 10 min to improve interlayer contact, yielding a sample with thickness of about 0.4 mm. It was found that the compressed “10-fold” sample could be folded for 2 more times (12 folds, Figure S3, Supporting Information).

However, this sample was not further studied in this work due to sample size constraints of the mechanical three-point bending testing equipment.

To make the composite with single layer graphene on one side of the PC film, the same PC solution was first spin-coated on the monolayer graphene film on Cu foil to form a **PCG** composite film, and then it was folded for 10 times in the same manner as described above. Large-scale CVD-grown polycrystalline graphene films on Cu foils were provided by the Chongqing Institute of Green and Intelligent Technology in Chinese Academy of Sciences (Figure S13, Supporting Information). The samples made with 400 nm thick PC, or 400 nm thick PC with monolayer graphene film were: i) 10-fold pure PC films (**F-PC**; thus having 1024 layers), ii) 10-fold **PCG** films (**F-PCG**; thus having 1024 layers), iii) 1024 stacked layers of PC film (**S-PC**), and iv) 1024 stacked layers of **PCG** film in a PCG–GPC manner (**S-PCG**). All of these types of samples were hot pressed at 150 °C for 10 min at  $\approx 40$ MPa to remove gaps between each layer. 5 separate samples of each type i)–iv) were made with the same procedure so that the mechanical testing could account for experimental variance.

**Characterizations:** A Bruker Dimension Icon AFM instrument was used to analyze the thickness of the single layer **PCG** film. Raman spectroscopy was done with a Wi-Tec micro-Raman instrument using a 532 nm laser excitation with a spot size of 250 nm. A FEI Verios 460 SEM was used to observe the structures of the composites. A three-point bending test configuration on a dynamic mechanical analyzer (DMA Q800, TA Instruments) was done to measure the bending response of the composite samples. The

dimensions of the specimens were  $15 \text{ mm} \times \approx 1.1 \text{ mm} \times \approx 0.4 \text{ mm}$  (span  $\times$  width  $\times$  thickness). The stress–strain plots were obtained with a displacement rate of  $100 \text{ } \mu\text{m min}^{-1}$  and the applied force and deflection were measured.

**FEM modeling:** FEM simulations replicating the three-point bending test configuration were performed to discriminate and quantify the restrain role of folding on the scaling of bending properties, independently from the material used. The material was PC following a linear elastic and isotropic constitutive behavior ( $E = 2.2 \text{ GPa}$ ,  $\nu = 0.37$ ,  $\rho = 1.21 \text{ g cm}^{-3}$ ). The simulated plate had planar dimensions of  $5.0 \times 3.5 \text{ mm}^2$ . The plate was supported by two rigid cylinders of radius  $0.2 \text{ mm}$  with axes orthogonal to the plate longest edge and at a mutual distance (span) of  $3 \text{ mm}$ . The load at the mid-span was applied by a third rigid cylinder (radius  $0.2 \text{ mm}$ ) moving at a constant imposed velocity of  $1 \text{ mm min}^{-1}$  up to a total deflection of  $1 \text{ mm}$ . Contact algorithm was implemented between the rigid cylinder and the layers and between each layer. A conventional coefficient of friction  $\mu = 0.31$  was assumed, which is an ordinary value for PC. Each layer was made of thick-shell elements with thickness  $8 \text{ } \mu\text{m}$  (in plane dimension  $50 \times 50 \text{ } \mu\text{m}^2$ , aspect ratio 6.25) with one element through the thickness. This thickness value was the lowest that could be simulated in order to have correct contact detection and stability with the used discretization. Because of the extremely long time scale, the real fold process could not be simulated. Folds were taken into account by welding together the edge nodes of different layers in the correspondence of folds (e.g., for 1 fold, the nodes at one edge were welded, for 2 folds, 4 layers were welded at one edge, 2 couples of 2 layers each were welded at another edge, no

constraint at the other edges, etc., as the reader may verify by folding a paper). To compare simulation results to experiments and theory, the bending properties were normalized with respect to the mass of the samples. Since the simulated experiment is in displacement control, the bending force was measured indirectly from the reactions at the two cylindrical supports whose sum, for static equilibrium, was equal to the external force applied by the moving cylinder. The bending stiffness was computed according to the three-point bending scheme as  $D_n = \frac{EI}{w} = \frac{PL^3}{48w\delta}$ .

### **Acknowledgements**

This work was supported by the Institute for Basic Science (Grant No. IBS-R019-D1). N.M.P. is supported by the European Commission under the Graphene Flagship Core 2 grant No. 785219 (WP14 “Polymer Composites”) and FET Proactive “Neurofibres” grant No. 732344 as well as by the Italian Ministry of Education, University and Research (MIUR) under the “Departments of Excellence” grant L.232/2016. The authors acknowledge financial support from the National Natural Science Foundation of China (Grant No. 51402291). S.S. acknowledges financial support from the BrainKorea21 Plus (National Science Foundation of Korea) and the Ermenegildo Zegna Founder’s Scholarship 2017–2018. This study was also supported by the Creative Materials Discovery Program (Grant No. 2016M3D1A1900038) through the National Research Foundation of Korea (NRF).

## References

- [1] Y. Zhu, H. Ji, H.-M. Cheng, R. S. Ruoff, *Natl. Sci. Rev.* **2017**, *5*, 90.
- [2] L. Gong, R. J. Young, I. A. Kinloch, I. Riaz, R. Jalil, K. S. Novoselov, *ACS Nano* **2012**, *6*, 2086.
- [3] H. Porwal, P. Tatarko, S. Grasso, J. Khaliq, I. Dlouhy, M. J. Reece, *Carbon* **2013**, *64*, 359.
- [4] M. Istrate, K. R. Paton, U. Khan, A. O'Neill, A. P. Bell, J. N. Coleman, *Carbon* **2014**, *78*, 243.
- [5] Nieto, R. Dua, C. Zhang, B. Boesl, S. Ramaswamy, A. Agarwal, *Adv. Funct. Mater.* **2015**, *25*, 3916.
- [6] J. J. Liang, Y. Huang, L. Zhang, Y. Wang, Y. F. Ma, T. Y. Guo, Y. S. Chen, *Adv. Funct. Mater.* **2009**, *19*, 2297.
- [7] G. Goncalves, P. Marques, A. Barros-Timmons, I. Bdkin, M. K. Singh, N. Emami, J. Gracio, *J. Mater. Chem.* **2010**, *20*, 9927.
- [8] S. Vadukumpully, J. Paul, N. Mahanta, S. Valiyaveetil, *Carbon* **2011**, *49*, 198.
- [9] P. May, U. Khan, A. O'Neill, J. N. Coleman, *J. Mater. Chem.* **2012**, *22*, 1278.
- [10] M. Z. Seyedin, J. M. Razal, P. C. Innis, R. Jalili, G. G. Wallace, *Adv. Funct. Mater.* **2015**, *25*, 94.
- [11] I. Alstrup, I. Chorkendorff, S. Ullman, *Surf. Sci.* **1992**, *264*, 95.
- [12] X. Li, W. Cai, J. An, S. Kim, J. Nah, D. Yang, R. Piner, A. Velamakanni, I. Jung, E. Tutuc, S. K. Banerjee, L. Colombo, R. S. Ruoff, *Science* **2009**, *324*, 1312.
- [13] A. Reina, X. Jia, J. Ho, D. Nezich, H. Son, V. Bulovic, M. S. Dresselhaus, J. Kong, *Nano Lett.* **2009**, *9*, 30.
- [14] S. Bae, H. Kim, Y. Lee, X. Xu, J.-S. Park, Y. Zheng, J. Balakrishnan, T. Lei, H. Ri Kim, Y. I. Song, Y.-J. Kim, K. S. Kim, B. Ozyilmaz, J.-H. Ahn, B. H. Hong, S. Iijima, *Nat. Nanotechnol.* **2010**, *5*, 574.
- [15] Y.-H. Lee, X.-Q. Zhang, W. Zhang, M.-T. Chang, C.-T. Lin, K.-D. Chang, Y.-C. Yu, J. T.-W. Wang, C.-S. Chang, L.-J. Li, T.-W. Lin, *Adv. Mater.* **2012**, *24*, 2320.

- [16] P. Liu, Z. Jin, G. Katsukis, L. W. Drahushuk, S. Shimizu, C.-J. Shih, E. D. Wetzel, J. K. Taggart-Scarff, B. Qing, K. J. Van Vliet, R. Li, B. L. Wardle, M. S. Strano, *Science* **2016**, 353, 364.
- [17] Vlassioun, G. Polizos, R. Cooper, I. Ivanov, J. K. Keum, F. Paulauskas, P. Datskos, S. Smirnov, *ACS Appl. Mater. Interfaces* **2015**, 7, 10702.
- [18] N. M. Pugno, *J. Mech. Phys. Solids* **2010**, 58, 1397.
- [19] B. C. Gallivan, *How to Fold Paper in Half Twelve Times: An Impossible Challenge Solved and Explained*, Historical Society of Pomona Valley, **2002**.
- [20] B. Wang, M. Huang, N. Y. Kim, B. V. Cunning, Y. Huang, D. Qu, X. Chen, S. Jin, M. Biswal, X. Zhang, S. H. Lee, H. Lim, W. J. Yoo, Z. Lee, R. S. Ruoff, *Nano Lett.* **2017**, 17, 1467.
- [21] B. Wang, M. Huang, L. Tao, S. H. Lee, A. R. Jang, B.-W. Li, H. S. Shin, D. Akinwande, R. S. Ruoff, *ACS Nano* **2016**, 10, 1404.
- [22] Z. C. Li, W. Zhang, X. Fan, P. Wu, C. Zeng, Z. Li, X. Zhai, J. Yang, J. Hou, *J. Phys. Chem. C*, **2012**, 116, 10557.
- [23] K. Kim, S. Coh, L. Z. Tan, W. Regan, J. M. Yuk, E. Chatterjee, M. F. Crommie, M. L. Cohen, S. G. Louie, A. Zettl, *Phys. Rev. Lett.* **2012**, 108, 246103.
- [24] C. S. Ruiz-Vargas, H. L. Zhuang, P. Y. Huang, A. M. van der Zande, S. Garg, P. L. McEuen, D. A. Muller, R. G. Hennig, J. Park, *Nano Lett.* **2011**, 11, 2259.
- [25] Q.-Y. Lin, G. Jing, Y.-B. Zhou, Y.-F. Wang, J. Meng, Y.-Q. Bie, D.-P. Yu, Z.-M. Liao, *ACS Nano* **2013**, 7, 1171.
- [26] C. Lee, X. Wei, J. W. Kysar, J. Hone, *Science* **2008**, 321, 385.
- [27] X. Chen, C. Yi, C. Ke, *Appl. Phys. Lett.* **2015**, 106, 101907.